

The effects of coating culture dishes with collagen on fibroblast cell shape and swirling pattern formation

Kei Hashimoto^{1,2,3,†}, Kimiko Yamashita^{1,2,4,5,†}, Kanako Enoyoshi^{1,2,†}, Xavier Dahan²,
Tatsu Takeuchi⁶, Hiroshi Kori^{1,7,*}, and Mari Gotoh³

¹Graduate School of Humanities and Sciences, Ochanomizu University, Ohtsuka,
Bunkyo-ku, Tokyo, Japan

²Program for Leading Graduate Schools, Ochanomizu University, Ohtsuka, Bunkyo-ku,
Tokyo, Japan

³Institute for Human Life Innovation, Ochanomizu University, Ohtsuka, Bunkyo-ku,
Tokyo, Japan

⁴Department of Physics, National Tsing Hua University, Hsinchu, Taiwan

⁵Physics Division, National Center for Theoretical Sciences, Hsinchu, Taiwan

⁶Department of Physics, Virginia Tech, Blacksburg, VA 24061, USA

⁷Department of Complexity Science and Engineering, Graduate School of Frontier
Sciences, The University of Toyo, Kashiwa, Japan

*Correspondence should be addressed to H. Kori (kori@k.u-tokyo.ac.jp)

Abstract

Motile human-skin fibroblasts form macroscopic swirling patterns when grown to confluence on a culture dish. In this paper, we investigate the effect of coating the culture-dish surface with collagen on the resulting pattern, using human-skin fibroblast NB1RGB cells as the model system. The presence of the collagen coating is expected to enhance the adherence of the fibroblasts to the dish surface, and thereby also enhance the traction that the fibroblasts have as they move. We find that, contrary to our initial expectation, the coating does not significantly affect the motility of the fibroblasts. Their eventual number density at confluence is also unaffected. However, the coherence length of cell orientation in the swirling pattern is diminished. We also find that the fibroblasts cultured in a collagen-coated dish are rounder in shape and shorter in perimeter, compared to those cultured in an uncoated dish. We hypothesize that the rounder cell-shape which weakens the cell–cell nematic contact interaction is responsible for the change in coherence length. A simple mathematical model of the migrating fibroblasts is constructed, which demonstrates that constant motility with weaker nematic interaction strength does indeed lead to the shortening of the coherence length.

Introduction

Collective cell migration is a key process observed at various stages in the development of multi-cellular organisms, starting with gastrulation and continuing into organogenesis¹. Well-studied examples include neural-tube closure of vertebrae, and lateral-line formation in zebrafish. After birth, it is involved in wound healing and cancer metastasis². Collective cell migration is also observed in single-cell organisms. A well-known example is aggregation by which *Dictyostelium* cells form a slug-like structure when starved³. Deciphering the mechanisms that drive robust and precise collective migration of large numbers of cells is of vital importance in understanding development, differentiation, and evolution, with many possible applications in cancer therapies, regenerative medicine, and tissue engineering^{2,4,5,6}.

In vitro cultivation studies can provide important insights into collective cell migration. When the cells are cultivated densely, complex alignment patterns spontaneously form in several cases. The characteristic coherence length of the alignment pattern is of special interest since it provides a measure of the number of cells that can migrate collectively. One of the key factors determining the coherence length is the strength of the cell–cell contact interaction. Although a migrating cell has vectorial polarity, moving toward a specific heading, the alignment of these cells is often nematic, that is, neighbouring cells tend to migrate either in parallel or anti-parallel directions. This nematic alignment can be observed in several cellular-scale objects including gliding microtubules, actin filaments, bacteria, and cultured cells⁷⁻¹⁰. Nematic alignment is also observed in purely mechanical systems whose members interact via the excluded-

volume effect, such as in a population of rod-like objects¹¹. In this case, the strength of the nematic interaction is determined by the shape of the rods; the interaction being stronger between longer rods.

In the present paper, we investigate the alignment pattern of human-skin fibroblast NB1RGB cells grown to confluence in a polystyrene culture dish. Skin-fibroblasts are cells that provide structural support for the skin and are easily cultivated *in vitro*. They represent a convenient model system for studying the collective migration of cells. Here, we examine how the alignment pattern depends on whether or not the dish surface is coated with collagen.

Since fibroblasts adhere to collagen via integrins, a natural expectation would be that the collagen-coated surface would provide enhanced traction to the fibroblasts leading to their enhanced motility, which in turn would lead to a change in the alignment pattern. *In vitro*, the collagenous extracellular matrix (ECM) is known to stimulate skin-fibroblast motility¹², which adds support to this expectation.

When fibroblasts are seeded onto a culture dish at low density, the cells adhere to the dish individually and then migrate randomly into cell-free areas while only occasionally coming into contact with other cells. As they proliferate, their density increases and confluence is eventually achieved. Confluent fibroblasts align locally along their elongated axes and form macroscopic swirling patterns. (See Supplementary Videos 1 and 2; not available in this preprint). A similar swirling pattern, the storiform pattern, is often observed in fibrohistiocytic lesions *in vivo*^{13,14}.

We find that the characteristic coherence length of the pattern decreases as the density of the collagen coated onto the culture dishes is increased. Moreover, we observe that the cells become rounder in shape with the increase in coated-collagen density, whereas cell-number density and, unexpectedly, cell motility remain unchanged. From these experimental results, we hypothesize that the difference in the coherence length mainly follows from the difference in the strength of the nematic contact interaction between the cells; i.e., rounder cells experience weaker nematic interactions, and thereby the coherence length becomes shorter. To test the feasibility of this hypothesis, we construct a simple mathematical model of migrating cells in which the strength of the nematic interaction can be controlled by a single parameter. Numerical simulations of this model demonstrate that the coherence length does indeed correlate positively with the nematic interaction strength. We thus propose that the collagen coating first leads to the change in the fibroblast cell-shape, which in turn shortens the coherence length. Possible mechanisms in which the collagen coating leads to the rounding of the fibroblasts is also discussed.

Results

Human-skin fibroblast NB1RGB cells form macroscopic swirling patterns

Human-skin fibroblast NB1RGB cells form macroscopic swirling patterns when cultivated in a culture dish due to their elongated shape, motility, and proliferation

within the confined two-dimensional surface. Our objective is to quantify the difference in the swirling patterns when the fibroblasts are cultured on uncoated, and collagen-type-I-coated dishes (polystyrene). The collagen-coating procedure is detailed in the Materials and Methods section. The resulting collagen density on the surface of the culture dish depends on the concentration of collagen type-I in the initial collagen solution used in the coating process. We use the coating obtained from a 10.0 $\mu\text{g}/\text{mL}$ collagen type-I solution as the standard reference.

Typical results for the uncoated and collagen-coated cases are shown in Fig. 1A. See also Supplementary Videos 1 (uncoated) and 2 (collagen-coated) (not available in this preprint). In the first row of Fig. 1A, still images of the confluent fibroblast patterns on uncoated (left) and collagen-coated (right) dishes are shown. The black scale bar in the lower-right corner of the right image is 1 mm long. For ease of comparison, the orientations of the individual fibroblasts in these images are read using Orientation J software¹⁵ and shown colour-coded in the second row of Fig. 1A, with light-blue and red respectively indicating horizontal and vertical orientations. Other colours indicate orientations in between, as shown on the scale to the right of Fig. 1B.

Comparing the colour-coded images by inspection, one discerns that the fibroblasts form into patches of cells with similar orientation, and that these patches are slightly larger for the uncoated dish compared to the collagen-coated dish.

We quantify this observation by extracting the correlations of cell orientations from the images as follows. First, the 1600×1200 pixel image is divided into a 50×38 grid,

each subdivision being 32×32 pixels in size. Then, the block-averaged orientation of the fibroblasts is calculated for each subdivision, the results of which are shown in Fig. 1B.

The correlations between the block-averaged orientations for each separation of the blocks is then calculated. The procedure is explained in detail in Materials and Methods. The resulting correlation functions are plotted in Fig. 1C (uncoated) and 1D (collagen-coated) for the images shown in Fig. 1A. A blow-up of the graphs between 0 to 1 mm is shown in the subframe inside Fig. 1D (labelled C' and D'). We can see that the orientation correlation falls off more quickly for the collagen-coated dish compared to the uncoated dish. This difference was consistently reproduced for multiple dishes, over multiple repetitions of the experiment.

To characterise the fall-off of the correlation function with distance, we define the lengths d_{50} and d_{20} to be the distances where the correlation is respectively reduced to half (50%) and to a fifth (20%) of the maximum value (100%). How these lengths are determined is illustrated in Figs. 1C and 1D. The values of d_{50} and d_{20} are calculated following this procedure for 40 different dishes and averaged. These average values are plotted in Fig. 1E for the uncoated, and collagen-coated dishes coated from collagen solutions of concentrations at 0.1, 1.0 and 10.0 $\mu\text{g}/\text{mL}$.

A clear trend can be seen in Fig. 1E in which the orientation coherence length decreases with the initial collagen concentration, indicating that the cell orientations vary more rapidly with distance when the collagen coatings on the culture dishes are denser,

resulting in the cells forming more swirling patterns overall.

The culture dishes in this study are coated with collagen molecules dissolved in acidic conditions, and not with collagen fibrils. To test whether the structure of the collagen coating affects the coherence length, we culture the cells in dishes coated with various types of collagen, all starting from an acidic (pH 3.0) solution of concentration 10.0 $\mu\text{g/mL}$. These are:

1. Collagen type-I (the reference)
2. Heat-denatured collagen type-I
3. Gelatin, which comprise thermal denatured collagen fibrils,
4. Collagen type-IV, which is a non-fibrillar form of collagen.

In all of these cases, the values of d_{50} and d_{20} are decreased compared with those of the control (uncoated). See Figs. S2A through F. This indicates that the reduction of orientation coherence occurs independently of the structure of collagen.

Collagen coating affects cell shape, but not single-cell motility or cell-number density

To clarify the effects of the collagen coating on individual fibroblast cells, we analyse cell motility and cell-number density, both of which are likely to affect the alignment pattern^{16,17}. To investigate cell motility, we track the movements of individual cells cultured at low and high densities (Fig. 2A). At low density, the instantaneous velocity is slightly smaller for the collagen-coated dish compared to the uncoated dish, but not by a significant amount. At high cell density, the instantaneous velocities are

indistinguishable between the uncoated and collagen-coated cases. Moreover, we measure the number of cells in the high-density cultures, and find no significant difference in the numbers of cells (Fig. 2B).

We also analyse the effects of the collagen coating on the fibroblast cell shape. We measure the area S and perimeter L of each cell on uncoated and 0.1, 1.0, and 10.0 $\mu\text{g/mL}$ collagen type-I-coated dishes at low density (Figs. 2C and 2F), and quantify the cell roundness in terms of the circularity $4\pi S/L^2$. See Fig. 2E.

These measurements indicate that the NB1RGB fibroblasts become rounder and smaller as the density of the collagen on the coating is increased. The same tendency is observed for heat-denatured collagen type-I, gelatin, and collagen type-IV (Figs. S2G, H), which suggests that interactions with the collagen coating makes the shape of NB1RGB fibroblasts rounder and smaller. At high density, it is difficult to quantify the cell shape since the cell boundaries become difficult to discern (Fig. 2D).

Simulation: interaction strength increases autocorrelation

Among our observations, the only significant difference between the cells cultured in coated and uncoated dishes is in their shapes at low density. Although it is possible that the difference in the cell shape is not maintained at high density, the shape of isolated single cells is likely to affect the orientation dynamics in highly dense cell populations.

Motivated by previous studies on the collective dynamics of rod-like objects¹¹, we consider the hypothesis that the nematic interactions between the cells in collagen-coated dishes are weaker than those in the uncoated dishes due to the cells becoming rounder in the presence of collagen, and it is this weaker nematic interaction that leads to the shorter coherence length.

The viability of this hypothesis depends on whether varying the strength of nematic interactions alone is sufficient in changing the coherence length. To this end, we construct a simple mathematical model with just a few tunable parameters, as described in Materials and Methods, and perform numerical simulations to assess the effect of different nematic interaction strengths on the cell alignment patterns.

Despite its simplicity, our model reproduces the experimentally observed dynamical behaviour well. See Supplementary Videos 3 and 4 (not available in this preprint). Fig. 3 shows some typical numerical results, where the parameter K (in units of hour^{-1}) quantifies the strength of the nematic interaction. Fig. 3A is the alignment pattern obtained for $K = 0.035/\text{hour}$, Fig. 3C its block-averaged cell orientations, and Fig. 3E the corresponding distance dependence of the orientation correlation. Figs. 3B, 3D, and 3F are those for $K = 0.020/\text{hour}$.

As shown in Fig. 3G, an increase in the nematic interaction strength K results in an increase in coherence length. There, we also check the robustness of our numerical results against changes in migration velocity; changes in the d_{20} and d_{50} values on the

interaction strength are small for the range of migration velocities observed experimentally (Fig. 2A).

Our simple mathematical model thus demonstrates that the effect of collagen coating on the orientation patterns can be accounted for solely by collagen's effect on the strength of the nematic interactions between the fibroblast cells.

Discussion

Human-skin fibroblasts cultured at high density form macroscopic swirling patterns in the culture dishes. This study revealed that the cells become rounder and form less coherent patterns as the density of the collagen coated on culture dishes is increased.

There are clear differences in the morphological properties between cells cultured in the uncoated and coated dishes; cells cultured in the coated dishes are shorter in perimeter and rounder (Figs. 2C, E, F). The following molecular mechanism could underlie this change. It is known that the elongated cells have developed stress fibres; conversely, lamellipodia, which is an actin projection on the edge of cell, rather than a stress fibre, is activated to make the cells round¹⁸. Two members of the Rho GTPase family, RhoA and Rac1, are necessary for the regulation of various cellular behaviours, including microfilament network organisation. The formation of stress fibre and lamellipodia are induced by RhoA and Rac1, respectively¹⁹⁻²³. RhoA and Rac1 inhibit each other's activation, and this competition between the two is one of the factors that regulate cell morphogenesis^{19,24}. It has been reported that collagen type-I increases the activity of Rac1 in human platelets²⁵. In fibroblasts, it is unknown whether collagen controls the

Rac1 activity, whereas the inhibition of Rac1 activation promotes the expression of collagen protein, suggesting that collagen interacts with Rac1 in fibroblasts²⁶. Therefore, it is possible that the collagen coating induces the development of lamellipodia and decreases that of stress fibres *via* Rac1 activation, thus changing the NB1RGB cell roundness.

Collagen is also known to control fibroblast motility. Pozzi *et al.* reported that collagen coating promotes the cell migration into cell-free space using scratch assay²⁷. This result seemingly differs from our results shown in Fig. 2A, wherein no significant difference was found between the migration speeds in the uncoated and coated dishes. However, they do not contradict each other since the study of Pozzi *et al.* was not based on the instantaneous migration speed of individual cells, but on the long-term behaviour of the cell assembly. Moreover, the migration speed of individual cells may be sensitive to its measurement method, such as the discretisation of cell trajectories and the observation time-interval. Depending on the method, a significant difference between the uncoated and coated dishes could arise. However, our numerical simulations reveal that the coherence length is insensitive to small variations in migration velocity (Fig. 3G), suggesting that the difference in migration velocities at low density, if any actually exists, does not have a substantial effect on pattern formation at high density.

As the collagen density is increased, the cells become rounder, whereas cell motility remains unchanged, as shown in Figs. 1E and 2E. The same tendency is found for different types of coating materials (collagen type-I, heat-denatured collagen type-I, gelatin, and collagen type-IV), as shown in Fig. 2C. We thus hypothesise that the

change in coherence length results from a change in the cell–cell contact interactions mediated by a change in cell shape. However, we do not have any direct evidence of this, and it therefore remains an open issue. Use of genetic manipulation or inhibitors that exclusively control the cell shape would be required for such a study.

Concerning the mathematical models of fibroblast orientation proposed so far, some focus on the interplay between the cells and the extra-cellular matrix (ECM)^{28,29}, known as dynamic reciprocity. Fibroblast orientation has also been modelled in terms of individual cell migration³⁰. Systems of reaction-diffusion and integro-partial differential equations have also been used to model fibroblast orientation; however, these require large numbers of parameters and computational complexity that would unnecessarily complicate the isolation of the key target parameter. Instead, our goal in using mathematical modelling is to test the hypothesis that changes in the coherence length of the orientation patterns can be driven solely by changes in the strength of cell–cell interactions. We therefore considered a model in which the strength of the nematic interaction can be controlled by a single parameter. In addition, to keep the model as simple as possible, we regarded each cell as a self-driven particle with constant speed, following various theoretical studies on collective migration^{31,32}. Despite the simplicity of our model, it qualitatively reproduces our experimental findings (Fig. 3) and represented rather realistic dynamics of collective migration (Supplementary Videos 3 and 4; not available in this preprint). Our model thus demonstrates that the coherence length increases with the strength of the cell–cell interaction, lending support to our hypothesis.

Correlation analysis reveals that the patterns formed under the conditions of this experiment are on the order of several cell-lengths long; however, larger cell assemblies may migrate collectively *in vivo*³³. Possible factors that hamper larger scale coherence *in vitro* include noisy single-cell migration, cell division, and topological defects¹⁰. To realise the large-scale collective migration *in vivo*, several other factors may play substantial or complementary roles, such as cell adhesion, spontaneous role assignment among cells, and polarity alignments among adjacent cells³³⁻³⁵. Mechanical tension applied to the tissue would also contribute to collective migration^{36,37}.

Our experimental and numerical results support our hypothesis that cell shape affects large-scale coherence by mediating the strength of cell–cell contact interactions.

Although our finding is based on an *in vitro* system, such a mechanism may be at work *in vivo* as well. Thus, our study suggests that cell shape may play an essential role in cell–cell communication in single and multi-cellular organisms.

Materials and methods

Coating of culture dish

Collagen type-I, collagen type-IV, and gelatin were purchased from Nitta Gelatin Inc. (Osaka, Japan. Product names: Cellmatrix Type-I-A, Cellmatrix Type-IV, and GLS250).

Collagen type-I and type-IV are provided as acidic solutions of pH 3 and concentration 3 mg/mL. These were diluted with a 1 mM HCl solution (pH 3.0) to the desired concentrations. Gelatin was dissolved in the 1 mM HCl solution to the desired concentration. Maintaining the acidic condition prevents the formation of collagen fibrils from the collagen molecules. The heat-denatured collagen type-I solution was prepared by heating the 10.0 µg/ml Cellmatrix Type-I-A solution for 30 minutes at 60°C.

Cell culture dishes (polystyrene) (AS ONE, Osaka, Japan) were incubated with the various types of collagen solutions, or just the vehicle solution (1 mM HCl) for the uncoated control, overnight at 4°C. Subsequently, the dishes were air dried and washed four times in phosphate-buffered saline (PBS).

The amount of collagen that was attached to the dish surface was estimated as follows. Following the same procedure as the culture dishes, each well of a 96-well polystyrene plate was incubated with 50 µL of the collagen or vehicle solution overnight at 4°C, then air dried and washed four times in PBS. The amount of collagen attached to the well surface was then measured with the Collagen Quantitation Kit (Cosmo Bio, Tokyo, Japan) following the manufacturer's protocol.

By comparing the amount of coated collagen prepared with 1 and 10 µg/mL collagen solutions, we confirmed that the collagen coated on the wells increased approximately in proportion to the dosage (Fig. S1). Note that the detection limit of the Quantitation Kit was 0.4 µg/mL, thus the amount of collagen in the well prepared with 0.1 µg/mL

solution was below the detection limit.

Cell culture

Normal human-skin fibroblasts, RIKEN original (NB1RGB), were provided by the RIKEN BioResource Research Center through the National BioResource Project of MEXT, Japan.

The cells were cultured in minimum essential medium alpha (MEM α ; Life technologies, Carlsbad, CA) supplemented with 10% fetal bovine serum (FBS; Biowest, Nuaille, France) at 37°C in a humidified incubator with a 5% CO₂ atmosphere. The NB1RGB cells (5.0×10^5) were then plated onto the 100-mm diameter polystyrene dishes.

After 6 days of incubation, the cells were washed in ice-cold PBS and then fixed in ice-cold 100% methanol.

Images of 10 different fields from each culture dish were captured at $\times 50$ magnification with a digital microscope (VH-Z20W, KEYENCE, Osaka, Japan). Each image had 1600 \times 1200 pixels, corresponding to an area of $6960 \times 5220 \mu\text{m}^2$.

For the cell-number density measurements, the cells were dissociated from the dishes with 0.025% Trypsin-EDTA after the 6-day incubation, and the numbers of cells were counted using an automated cell counter (BACKMAN COULTER, Brea, CA). Color-coded maps were prepared using the orientation analysis plugin, OrientationJ, in ImageJ¹⁵. The Gaussian window was set to 1.5 pixels.

Average orientation images

Average orientation images were created to visualise the numerical orientation data collected by ImageJ with the plugin OrientationJ³⁸.

Each 1600×1200 -pixel image was subdivided into a 50×38 grid, each subdivision being 32×32 pixels ($139.2 \times 139.2 \mu\text{m}^2$) in size. Then, the block-averaged orientation was calculated for each of these subdivisions.

Correlation functions of orientation between fibroblasts

The correlation functions of orientation between the fibroblasts are computed as follows.

We label the subdivisions in the 50×38 grid with a pair of integers (k, ℓ) , where $1 \leq k \leq l_x = 50$, and $1 \leq \ell \leq l_y = 38$.

k labels the columns of the grid from left to right, while ℓ labels the rows of the grid from top to bottom.

The average orientation $\theta_{k\ell}$ of the fibroblasts in region (k, ℓ) is defined as the exponent appearing in the equation below:

$$R_{k\ell} e^{i2\theta_{k\ell}} = \frac{1}{N_{k\ell}} \sum_{j=0}^{N_{k\ell}-1} e^{i2\phi_j}$$

where i is the square root of -1 , $N_{k\ell}$ is the number of fibroblasts in region (k, ℓ) and ϕ_j is the angle of the j -th fibroblast with respect to the horizontal direction. Here, $R_{k\ell}$ measures the level of alignment of the cells within this region. It varies between 0 and 1, wherein values near 0 correspond to cases when orientations are extremely different, and those near 1 correspond to cases when orientations are almost the same. The

correlation between region (i, j) and region (k, ℓ) is defined as $C_{ij,k,\ell} = \cos 2(\theta_{ij} - \theta_{k\ell})$. The total correlation between region (i, j) and all other regions at distance d from region (i, j) is calculated as follows:

$$C_{ij}(d) = \sum_{(i-k)^2+(j-\ell)^2=d^2} C_{ij,k,\ell}$$

The correlation function $C(d)$ is computed as the average of this total correlation over all regions:

$$C(d) = \frac{1}{l_x l_y} \sum_{i=0}^{l_x-1} \sum_{j=0}^{l_y-1} C_{ij}(d)$$

The distance values d_{50} and d_{20} are defined as $C(d_{50}) = 0.5$ and $C(d_{20}) = 0.2$. Note that the distance d in these expressions is given in units of 32 pixels (139.2 μm) so it must be multiplied by 139.2 μm to convert to physical units.

Cell movies

To obtain high-resolution images, we used glass-bottom dishes (Iwaki Co., Ltd., Tokyo, Japan) along with high numerical aperture objective lens. The glass-bottom culture dishes were collagen-coated following the procedure described above from the 10.0 $\mu\text{g}/\text{mL}$ collagen type-I solution. Uncoated controls were prepared using only the vehicle solution (1 mM HCl) in the same procedure.

NB1RGB cells (6.0×10^4 cells/35-mm diameter dish) were seeded in the glass-bottom dishes, and were cultured for 90 h while taking time-laps images at 15-min intervals using a microscope (BZ-X700, KEYENCE, Osaka, Japan). See Supplementary Videos 1 and 2 (not available in this preprint).

The VW-H2MA motion analyser (KEYENCE), which performs cell tracking, was used to measure the cell migration velocity. The displacements of multiple cells during each 15-minute interval was measured, from which the average velocity of each cell during that time-interval (which is essentially the instantaneous velocity due to the cells moving slowly) was determined. This velocity was averaged over twenty cells. The velocities for low and high density conditions were respectively based on data from 0–30 h and 60–90 h after culture start.

The area S and perimeter L of the NB1RGB cells were measured using ImageJ after culturing for 30 h, and circularity was calculated as $4\pi S/L^2$.

Mathematical model

To obtain insight on the role of collagen in the 2D patterns formed by fibroblasts, we introduced a simple mathematical model of cell collective motion. The model equation is given as:

$$\frac{dx_i}{dt} = v \cos \theta_i + R_x(i) \quad (1)$$

$$\frac{dy_i}{dt} = v \sin \theta_i + R_y(i) \quad (2)$$

$$\frac{d\theta_i}{dt} = K \sum_j \exp\left(-\frac{r_{ij}^2}{2\lambda^2}\right) \sin 2(\theta_j - \theta_i) \quad (3)$$

where the variables $(x_i(t); y_i(t))$ and $\theta_i(t)$ are the position and the orientation of cell i at time t , respectively.

In this model, cell i migrates spontaneously in the direction $\theta_i(t)$ with constant speed v .

The terms R_x and R_y denote the repulsive force due to cell–cell excluded-volume interactions described as a Gaussian soft-core potential $H(r) = \sigma^2 K_c \exp\left(-\frac{r^2}{2\sigma^2}\right)$ with interaction strength K_c , distance r between cells, and typical cell length σ .

Explicitly, the terms R_x and R_y are given as:

$$R_x(i) = -\frac{\partial}{\partial x_i} \sum_j H(r_{ij}) = K_c \sum_j (x_i - x_j) \exp\left(-\frac{r_{ij}^2}{2\sigma^2}\right)$$

$$R_y(i) = -\frac{\partial}{\partial y_i} \sum_j H(r_{ij}) = K_c \sum_j (y_i - y_j) \exp\left(-\frac{r_{ij}^2}{2\sigma^2}\right)$$

where r_{ij} stands for the distance between cell i and cell j .

Equation (3) describes the nematic interaction with strength K between the cells that leads to the nematic alignment of cell orientations. A similar interaction was considered by Sumino Y. *et al.*⁷. The effective interaction strength in Equation (3) is $K \exp\left(-\frac{r_{ij}^2}{2\lambda^2}\right)$ with characteristic interaction length λ .

Simulation

The continuous-time model of Equations (1)–(3) was discretised for each cell using Euler’s method with a step size of 15 min, for a simulation length of 72 h (3 days), resulting in $72 \times 4 + 1 = 289$ frames.

To match the experimental data, each frame’s dimensions were adjusted to 69.6×52.2 units, where 1 unit is 100 μm . Instead of considering periodic boundaries, which would not match the experimental conditions, we added margins surrounding the frames in the

actual simulation. Each margin was 15 units wide, which was more than the distance travelled by a cell during the 72-h cultivation period (cell speed is ~ 0.18 unit/h $\times 72$ h ~ 13 units). Therefore, the actual frame dimensions for the simulation were 99.6×82.2 units. When creating the simulation video and while taking quantitative measurements for comparison with the experimental results, these margins were ignored.

The initial number of cells is $N_0 = 3434$, which corresponds to the initial cell density in the experiments, ~ 8000 cells/cm². All the simulated cells are initialised with random positions $(x_i(0), y_i(0))$ in the window and with a random orientation $\theta_i(0)$ in the range $[0, 2\pi)$. The increase in the cell number induced by cell divisions is set to 1.00491 cells/step (or 1.01979 cells/h) so that 14,080 cells result after 72 h of cultivation. Each new cell is divided from a randomly chosen existing cell, and is then positioned 1.392/4 units away from the origin cell and with the origin cell's orientation.

GIF animations from the 289 frames were generated using Gnuplot.

Correlation data were measured on the final, 289th image at $t = 72$ h, following the protocol described above for the experimental observations.

To correct for the effects of randomness in the simulation, 10 simulations with the same parameters were run and averaged data were reported as the simulation results.

Parameters

Soft-core Gaussian deviation (typical cell length): $\sigma = 0.696$ units.

Soft-core interaction strength: $K_C = 1.78/\text{h}$.

Gaussian deviation for the orientation characteristic interaction length: $\lambda = 0.696$ units.

The interaction strength K was varied from 0.010/h to 0.040/h.

Dependence of coherence length on migration speed

The simulations were conducted for the following three cases with regards to the constant speed v :

- 1) The measured migration velocity at low density on an uncoated dish: $v = 0.1864$ unit/h (1 unit = 100 μm , cf. Fig. 2A),
- 2) The measured migration velocity at low density on a coated dish: $v = 0.1598$ unit/h (cf. Fig. 2A),
- 3) The average of the above two: $v = 0.1731$ unit/h.

The dependence of the coherence length on these selections is shown in Fig. 3G.

The solid, dashed, and dotted lines are the average d_{20} and d_{50} values over ten simulations for cases 1), 2) and 3), respectively. The error bars are the standard deviation of 10 runs for case 1).

Statistical analyses

The data were analysed with a one-tailed Student's t -test. The values were expressed as the mean \pm mean standard error. Changes were considered to be significant if the p value from the Student's t -test was less than 0.05.

Acknowledgements

This work was supported by grants from the Leading Graduate School Promotion Center, Ochanomizu University. We are grateful to Dr. Khayrul Bashar, Dr. Kyogo Kawaguchi and Dr. Kyohei Shitara for their helpful advice. We are also grateful to Dr. Daiki Nishiguchi for providing the ImageJ script for automatic image analysis.

K.Y. acknowledges support from the Leading Graduate School Promotion Center of Ochanomizu University for a long-term stay at Virginia Tech; she thanks Professor John Tyson and his Computational Cell Biology Lab at Virginia Tech for their warm hospitality and the valuable advice she received while this work was conducted. M.G. acknowledges the financial support from JSPS KAKENHI Grant No. 26860144. H.K. acknowledges the financial support from MEXT KAKENHI Grant No. 15H05876 and JSPS KAKENHI Grant No. 18K11464.

Author contributions

H.K. and M.G. designed the study. K.H. and M.G. performed the experiments. H.K. constructed the mathematical model. K.Y. and X.D. conducted the simulations. H.K., T.T. and K.Y. constructed the method for obtaining the correlation of orientation and K.Y. implemented it. K.E and K.H. performed statistical analysis. K.H. wrote the initial draft of the manuscript, and K.E, K.Y., X.D., T.T., H.K and M.G. finalised the manuscript. All authors approved the final version of the manuscript.

Additional information

Competing financial interests: The authors declare no competing financial interests.

Figures

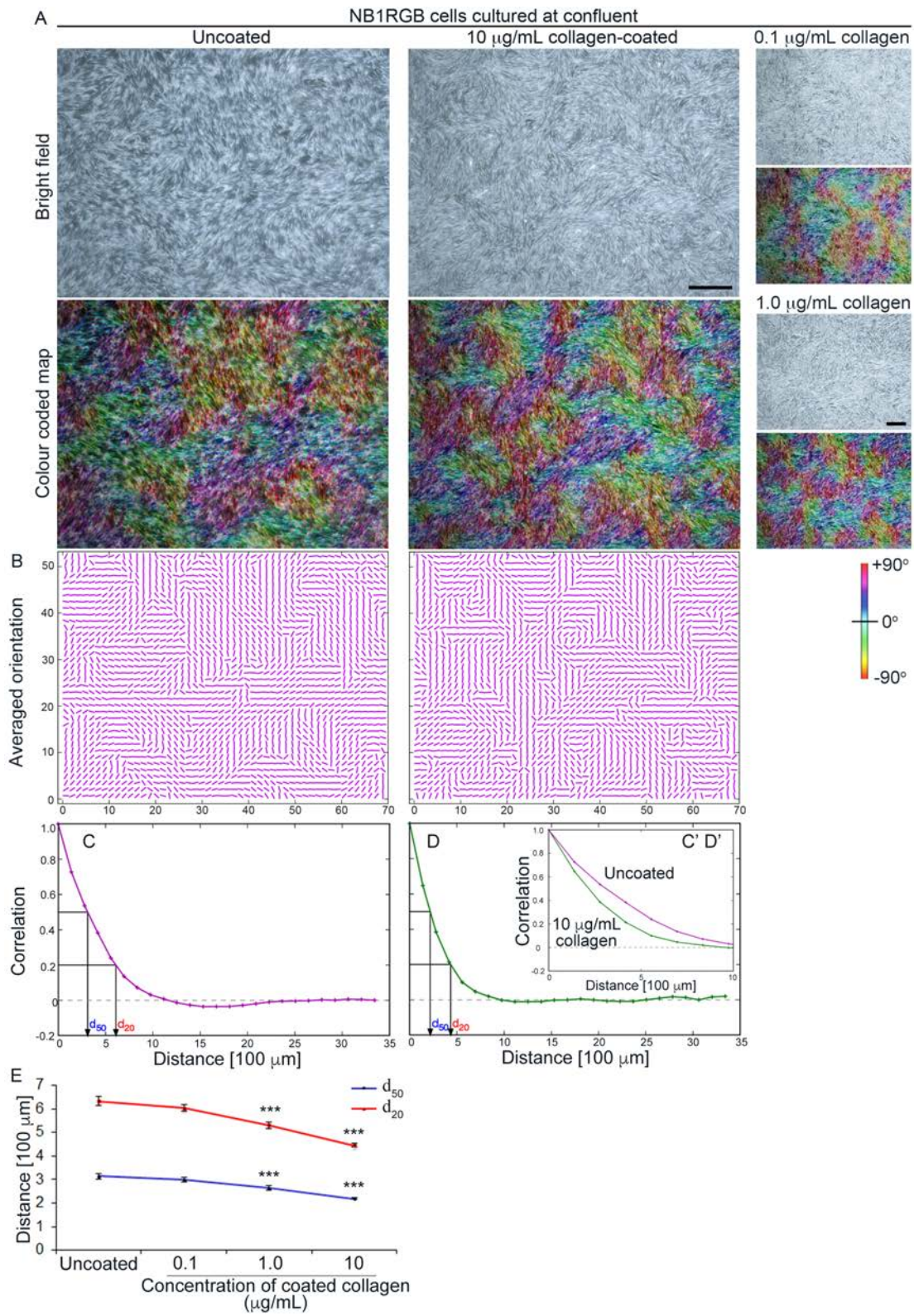


Figure 1 Patterns formed by human-skin NB1RGB fibroblast cells cultured in a dish.

A: Typical patterns of confluent fibroblast culture on the uncoated control (left) and the dish coated using the 10.0 $\mu\text{g}/\text{mL}$ collagen type-I solution (right). The black scale bar in the lower-right corner of the right-monochrome image is 1 mm long. The smaller images in the right-margin are for dishes coated from 0.1 $\mu\text{g}/\text{mL}$ (top) and 1.0 $\mu\text{g}/\text{mL}$ (bottom) collagen type-I solutions. For each pair of images, the lower colour-map encodes the orientations of the fibroblasts in the upper bright-field image in accordance with the colour-scale shown to the right of B. B: The block-averaged orientations of the fibroblasts on uncoated (left) and 10.0 $\mu\text{g}/\text{mL}$ collagen-coated (right) dishes shown in A. C: Correlation function of cell orientation for the uncoated, and D: collagen-coated cases. The graphs C' and D' in the sub-window show the behaviour of the two functions near the origin on the same axes for the ease of comparison. E: d_{20} and d_{50} values averaged over 40 images. Data represent the mean \pm standard error of the mean (SEM) of 40 images of the four types of culture dish coatings. Data points labelled with a triple asterisk (***) indicate points for which $p < 0.001$ under Student's one-tailed t -test.

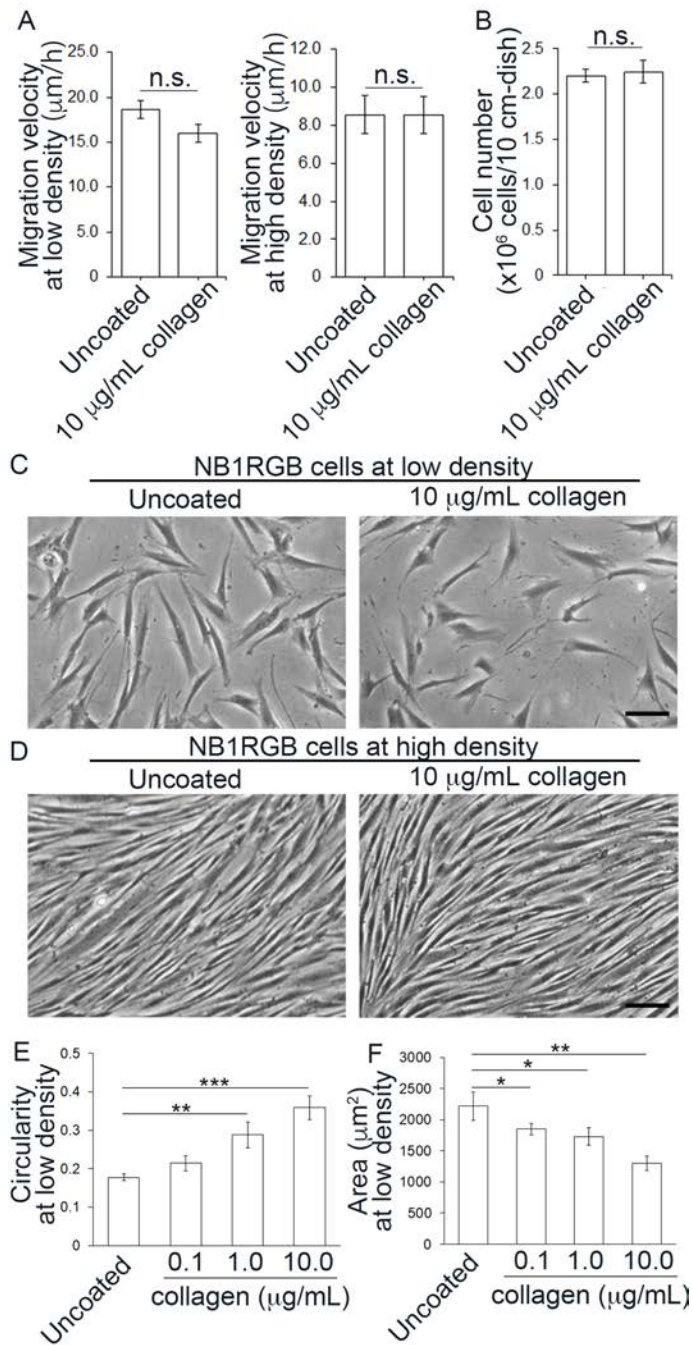


Figure 2 Collagen coating changes the morphology of the human-skin fibroblast cells rather than their mobility or density. A: Migration velocities of the fibroblasts cultured at low and high densities on uncoated and 10.0 $\mu\text{g}/\text{mL}$ collagen type-I-coated dishes. B: Number of fibroblasts at confluence on uncoated and 10 $\mu\text{g}/\text{mL}$ collagen type-I-coated dishes. (C-E) Analysis of fibroblast cell morphology. (C, D) Fibroblasts cultured on

uncoated and 10 $\mu\text{g}/\text{mL}$ collagen type-I-coated dishes at 30 h (C) and 90 h after culture start (D). Scale bar: 100 μm . (E, F) Circularity and area of fibroblasts cultured on uncoated and 0.1, 1.0, and 10.0 $\mu\text{g}/\text{mL}$ collagen type-I coated dishes at low density. The asterisks on the data points indicate *t*-test *p* values. *: $p < 0.05$, **: $p < 0.01$, ***: $p < 0.001$. Cell-count data represent the mean \pm SEM from nine experiments. Other data represent the mean \pm SEM of 20 cells sampled from two experiments.

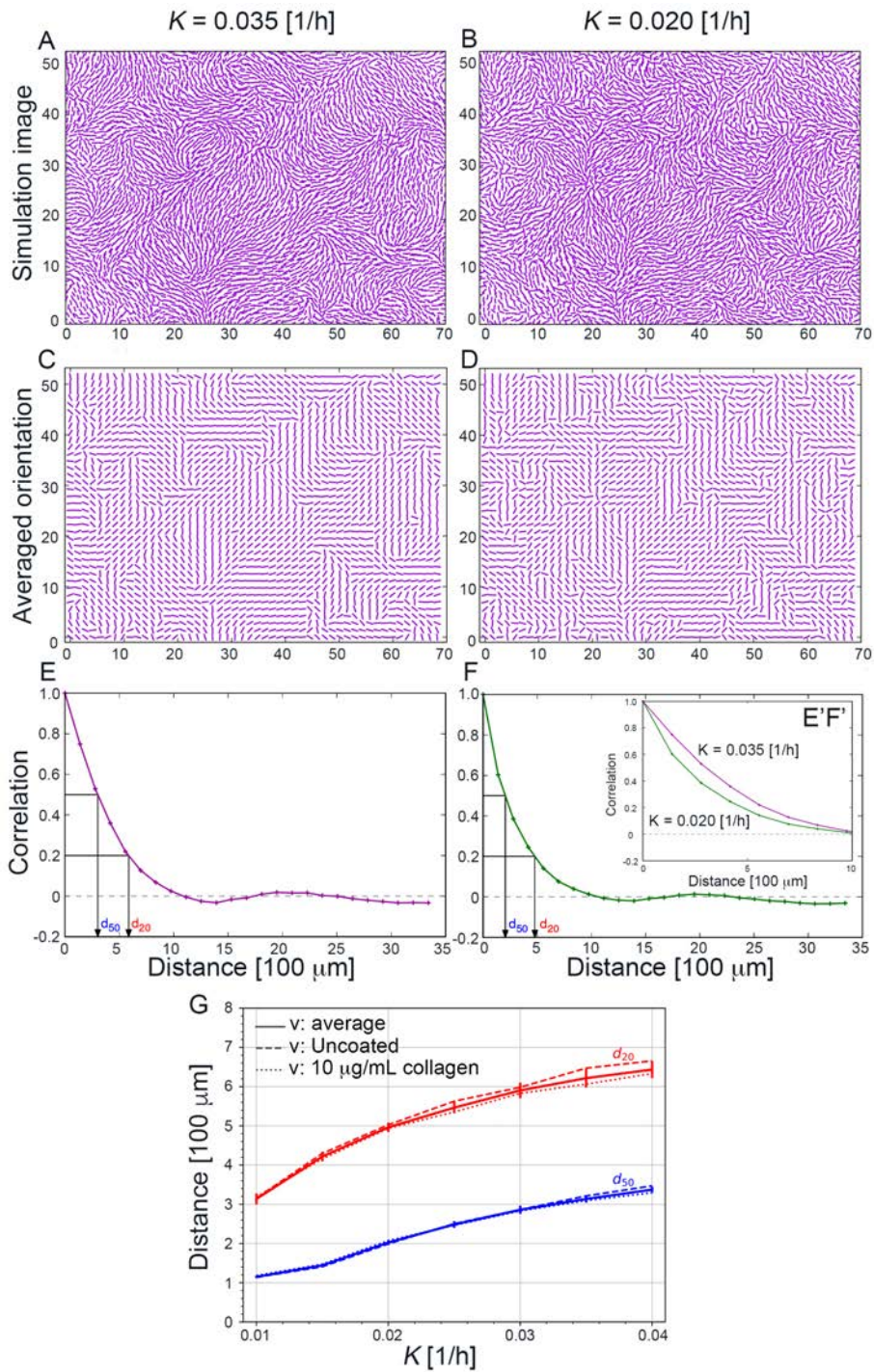


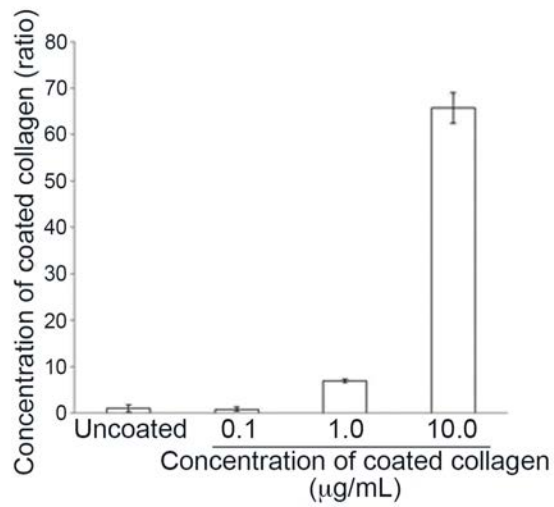
Figure 3 Simulation results correspond to $t = 72$ h. The strength of nematic interaction is $K = 0.035/\text{h}$ and $K = 0.020/\text{h}$ in (A, C, E) and (B, D, F), respectively. (A, B) Cell positions and orientations. (C, D) Averaged orientation for each 32×32 pixel box is shown. (E, F, E'F') Correlation value of cell orientations is shown with respect to a

distance between averaged cell orientations. (E) $K = 0.035/\text{h}$ and (F) $K = 0.020/\text{h}$. Both lines in (E'F') with shorter distance are up to 10 units. (G) Dependence of d_{20} and d_{50} on the interaction strength K . Solid lines correspond to $\nu = 0.1731$ unit/h (average), dashed lines to $\nu = 0.1864$ unit/h (uncoated measured value), and dotted lines to $\nu = 0.1598$ unit/h (10 $\mu\text{g}/\text{mL}$ collagen type-I-coated measured value). Each value of d_{20} and d_{50} is averaged over 10 simulations with respect to each point of K . For the $\nu = 0.1731$ unit/h (average) case, error bars are shown for the each point.

SUPPLEMENTARY INFORMATION

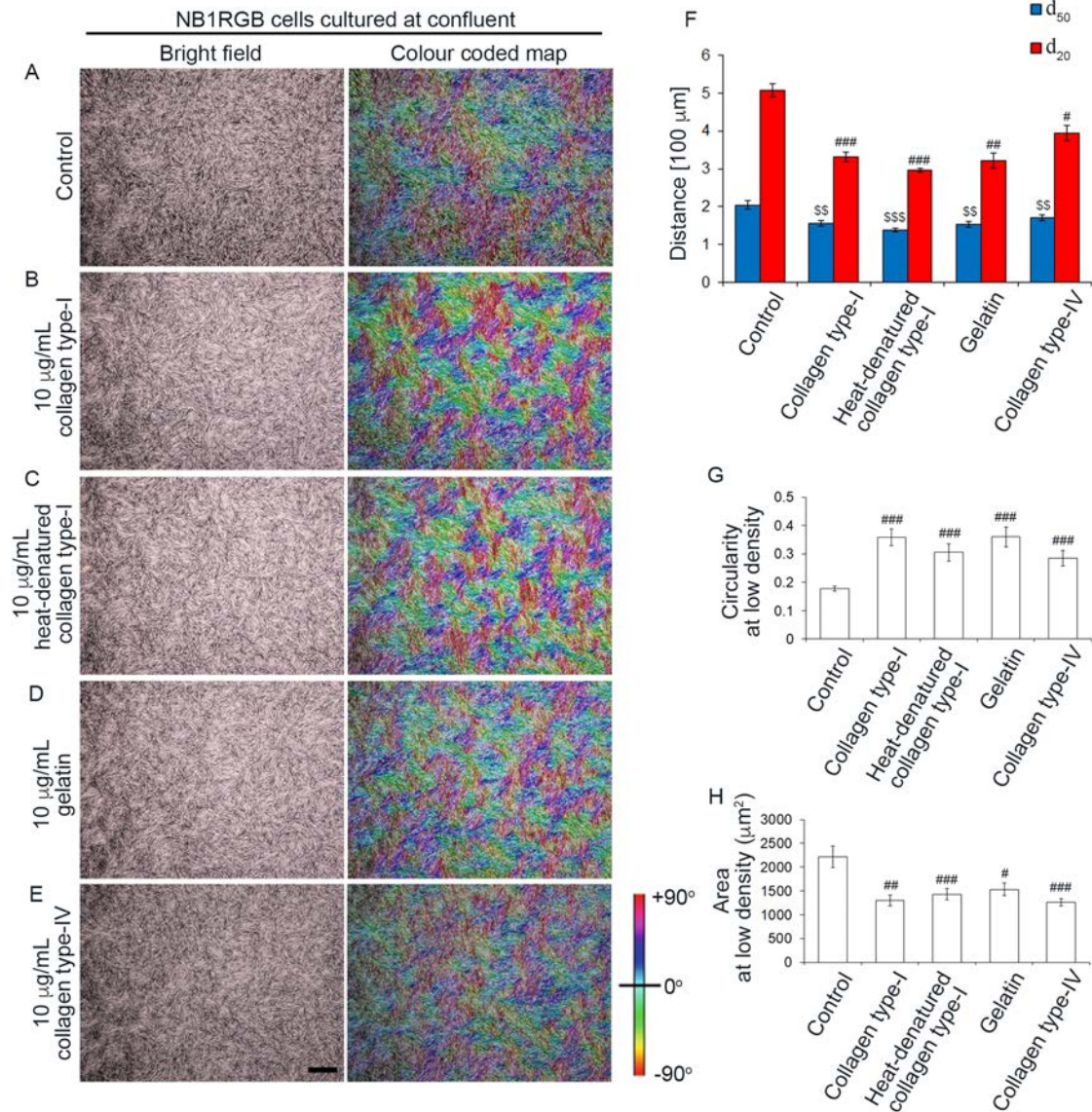
The effects of coating culture dishes with collagen on fibroblast cell shape and swirling pattern formation

Kei Hashimoto, Kimiko Yamashita, Kanako Enoyoshi, Xavier Dahan, Tatsu Takeuchi,
Hiroshi Kori*, Mari Gotoh



Supplementary Figure S1

The concentration of coated collagen on the well surface. The ratio of coated collagen type-I concentration on the well after incubating with 0 (uncoated control, only the 1 mM HCl vehicle solution), 0.1, 1.0 and 10.0 µg/mL collagen type-I solutions. The concentrations are normalized to that of the uncoated well. Data represent the mean \pm SEM for each of the four initial collagen concentrations.



Supplementary Figure S2

The effects of various types of collagen on the pattern formation of cultured human-skin fibroblasts, NB1RGB. (A–E) Bright-field images and colour coded maps of cultured NB1RGB cells at confluence on uncoated (control) (A), 10.0 µg/mL collagen type-I-coated (B), 10.0 µg/mL heat-denatured collagen type-I-coated (C), 10.0 µg/mL gelatin-coated (D), and 10.0 µg/mL collagen type-IV-coated (E) dishes. Scale bar: 1 mm. (F) d_{20} and d_{50} values. \$\$: $p < 0.01$, \$\$\$: $p < 0.001$, t -test vs. the d_{20} value of control, #: p

< 0.05, ##: $p < 0.01$, ###: $p < 0.001$, t -test vs. the d_{50} value of control. *: $p < 0.05$, t -test.

(G, H) Circularity and area of NB1RGB cultured at low density. #: $p < 0.05$, ##: $p <$

0.01, ###: $p < 0.001$, t -test vs. control value. *: $p < 0.05$, t -test. Correlation data

represent the mean \pm SEM of four images. Other data represent the mean \pm SEM of 20

cells.

Supplementary video legends (not available in this preprint)

Video 1 Experimentally obtained time courses of cell growth and migration on the uncoated dish.

Video 2 Experimentally obtained time courses of cell growth and migration on the 10 $\mu\text{g/mL}$ collagen type-I-coated dish.

Video 3 Numerically obtained time courses of cell growth and migration for $K = 0.035/\text{h}$.

Video 4 Numerically obtained time courses of cell growth and migration for $K = 0.020/\text{h}$.

References

- 1 Weijer, C. J. Collective cell migration in development. *J Cell Sci* **122**, 3215-3223, doi:10.1242/jcs.036517 (2009).
- 2 Ilin, O. & Friedl, P. Mechanisms of collective cell migration at a glance. *J Cell Sci* **122**, 3203-3208, doi:10.1242/jcs.036525 (2009).
- 3 Devreotes, P. Dictyostelium discoideum: a model system for cell-cell interactions in development. *Science* **245**, 1054-1058 (1989).
- 4 Carter, S. B. Haptotaxis and the mechanism of cell motility. *Nature* **213**, 256-260, doi:10.1038/213256a0 (1967).
- 5 Lauffenburger, D. A. & Horwitz, A. F. Cell migration: a physically integrated molecular process. *Cell* **84**, 359-369, doi:10.1016/s0092-8674(00)81280-5 (1996).
- 6 Li, L., He, Y., Zhao, M. & Jiang, J. Collective cell migration: Implications for wound healing and cancer invasion. *Burns Trauma* **1**, 21-26, doi:10.4103/2321-3868.113331 (2013).
- 7 Sumino, Y. *et al.* Large-scale vortex lattice emerging from collectively moving microtubules. *Nature* **483**, 448-452, doi:10.1038/nature10874 (2012).
- 8 Nishiguchi, D., Nagai, K. H., Chate, H. & Sano, M. Long-range nematic order and anomalous fluctuations in suspensions of swimming filamentous bacteria. *Phys Rev E* **95**, 020601, doi:10.1103/PhysRevE.95.020601 (2017).
- 9 Popp, D., Yamamoto, A., Iwasa, M. & Maeda, Y. Direct visualization of actin nematic network formation and dynamics. *Biochem Biophys Res Commun* **351**, 348-353, doi:10.1016/j.bbrc.2006.10.041 (2006).
- 10 Kawaguchi, K., Kageyama, R. & Sano, M. Topological defects control collective dynamics in neural progenitor cell cultures. *Nature* **545**, 327-331, doi:10.1038/nature22321 (2017).
- 11 Peruani, F., Deutsch, A. & Bar, M. Nonequilibrium clustering of self-propelled rods. *Phys Rev E Stat Nonlin Soft Matter Phys* **74**, 030904, doi:10.1103/PhysRevE.74.030904 (2006).
- 12 Li, W. *et al.* Mechanism of human dermal fibroblast migration driven by type I collagen and platelet-derived growth factor-BB. *Mol Biol Cell* **15**, 294-309, doi:10.1091/mbc.E03-05-0352 (2004).
- 13 Meister, P., Konrad, E. & Hohn, N. Incidence and histological structure of the storiform pattern in benign and malignant fibrous histiocytomas. *Virchows Arch A Pathol Anat Histol* **393**, 93-101 (1981).
- 14 Nakamura, I. *et al.* A Novel Chromosomal Translocation Associated With COL1A2-PDGFB Gene Fusion in Dermatofibrosarcoma Protuberans: PDGF Expression as a New Diagnostic Tool. *JAMA Dermatol* **151**, 1330-1337, doi:10.1001/jamadermatol.2015.2389 (2015).

- 15 Puspoki, Z., Storath, M., Sage, D. & Unser, M. Transforms and Operators for Directional Bioimage Analysis: A Survey. *Adv Anat Embryol Cell Biol* **219**, 69-93, doi:10.1007/978-3-319-28549-8_3 (2016).
- 16 Yang, Y. *et al.* Probing Leader Cells in Endothelial Collective Migration by Plasma Lithography Geometric Confinement. *Sci Rep* **6**, 22707, doi:10.1038/srep22707 (2016).
- 17 Vitorino, P. & Meyer, T. Modular control of endothelial sheet migration. *Genes Dev* **22**, 3268-3281, doi:10.1101/gad.1725808 (2008).
- 18 Tojkander, S., Gateva, G. & Lappalainen, P. Actin stress fibers--assembly, dynamics and biological roles. *J Cell Sci* **125**, 1855-1864, doi:10.1242/jcs.098087 (2012).
- 19 Rottner, K. & Stradal, T. E. Actin dynamics and turnover in cell motility. *Curr Opin Cell Biol* **23**, 569-578, doi:10.1016/j.ceb.2011.07.003 (2011).
- 20 Ridley, A. J. & Hall, A. The small GTP-binding protein rho regulates the assembly of focal adhesions and actin stress fibers in response to growth factors. *Cell* **70**, 389-399 (1992).
- 21 Hall, A. Rho GTPases and the actin cytoskeleton. *Science* **279**, 509-514 (1998).
- 22 Amano, M. *et al.* Formation of actin stress fibers and focal adhesions enhanced by Rho-kinase. *Science* **275**, 1308-1311 (1997).
- 23 Nobes, C. D. & Hall, A. Rho, rac, and cdc42 GTPases regulate the assembly of multimolecular focal complexes associated with actin stress fibers, lamellipodia, and filopodia. *Cell* **81**, 53-62 (1995).
- 24 Rottner, K., Hall, A. & Small, J. V. Interplay between Rac and Rho in the control of substrate contact dynamics. *Curr Biol* **9**, 640-648 (1999).
- 25 Kageyama, Y. *et al.* Rac regulates collagen-induced HSP27 phosphorylation via p44/p42 MAP kinase in human platelets. *Int J Mol Med* **32**, 813-818, doi:10.3892/ijmm.2013.1455 (2013).
- 26 Igata, T. *et al.* Up-regulated type I collagen expression by the inhibition of Rac1 signaling pathway in human dermal fibroblasts. *Biochem Biophys Res Commun* **393**, 101-105, doi:10.1016/j.bbrc.2010.01.090 (2010).
- 27 Pozzi, A., Wary, K. K., Giancotti, F. G. & Gardner, H. A. Integrin alpha1beta1 mediates a unique collagen-dependent proliferation pathway in vivo. *J Cell Biol* **142**, 587-594 (1998).
- 28 Dallon, J. C. & Sherratt, J. A. A mathematical model for fibroblast and collagen orientation. *Bull Math Biol* **60**, 101-129, doi:10.1006/bulm.1997.0027 (1998).
- 29 Dallon, J. C., Sherratt, J. A. & Maini, P. K. Mathematical modelling of extracellular matrix dynamics using discrete cells: fiber orientation and tissue regeneration. *J Theor Biol* **199**, 449-471, doi:10.1006/jtbi.1999.0971 (1999).
- 30 Painter, K. J. Modelling cell migration strategies in the extracellular matrix. *J Math Biol* **58**, 511-543, doi:10.1007/s00285-008-0217-8 (2009).
- 31 Vicsek, T., Czirok, A., Ben-Jacob, E., Cohen, I. I. & Shochet, O. Novel type of phase transition in a system of self-driven particles. *Phys Rev Lett* **75**, 1226-1229, doi:10.1103/PhysRevLett.75.1226

- (1995).
- 32 Chat'é, H., Ginelli, F., Gr'egoire, G., Peruani, F. & Raynaud, F. Modeling collective motion: variations on the Vicsek model. *The European Physical Journal B* **64**, 451–456 doi:10.1140/epjb/e2008-00275-9 THE (2008).
- 33 Mayor, R. & Etienne-Manneville, S. The front and rear of collective cell migration. *Nat Rev Mol Cell Biol* **17**, 97-109, doi:10.1038/nrm.2015.14 (2016).
- 34 Theveneau, E. *et al.* Collective chemotaxis requires contact-dependent cell polarity. *Dev Cell* **19**, 39-53, doi:10.1016/j.devcel.2010.06.012 (2010).
- 35 Devenport, D. The cell biology of planar cell polarity. *J Cell Biol* **207**, 171-179, doi:10.1083/jcb.201408039 (2014).
- 36 Aw, W. Y. & Devenport, D. Planar cell polarity: global inputs establishing cellular asymmetry. *Curr Opin Cell Biol* **44**, 110-116, doi:10.1016/j.ceb.2016.08.002 (2017).
- 37 Sugimura, K. & Kori, H. A reduced cell-based phase model for tissue polarity alignment through global anisotropic cues. *Sci Rep* **7**, 17466, doi:10.1038/s41598-017-17611-8 (2017).
- 38 Fonck, E. *et al.* Effect of aging on elastin functionality in human cerebral arteries. *Stroke* **40**, 2552-2556, doi:10.1161/STROKEAHA.108.528091 (2009).